EFFECT OF THERMAL RADIATION ON UNSTEADY MIXED CONVECTION FLOW NEAR FORWARD STAGNATION POINT OVER A CYLINDER OF ELLIPTIC CROSS-SECTION

by

Tariq JAVED, Irfan MUSTAFA*, and Hussain AHMAD

Department of Mathematics and Statistics, FBAS, International Islamic University, Islamabad, Pakistan

Original scientific paper
DOI:10.2298/TSCI140926027J

The effect of thermal radiation on unsteady mixed convection flow near a forward stagnation point over a cylinder of elliptic cross-section is investigated in this paper. The governing equations are transformed into dimensionless partial differential equations by using a suitable transformation and then solved numerically by using an implicit finite difference scheme known as Keller Box method. The accuracy of the results is verified by comparing the obtained results with the previous studies available in the literature. It is shown that the results are highly accurate and are in good agreement. The separation times for both blunt and slender orientations in the presence of thermal radiation are shown in tabular forms. Moreover, the effects of pertinent parameters including Prandtl number, mixed convection parameter, thermal radiation parameter, surface temperature parameter, and blunt/slender orientation parameter ω on the velocity profile, the temperature profile and the Nusselt number also are shown graphically. From the present study, it is observed that boundary layer separation occurs early due to thermal radiation and Nusselt number increases for both blunt and slender orientations.

Key words: *thermal radiation, unsteady mixed convection flow, forward stagnation point, elliptic cylinder*

Introduction

Study of mixed convection flow has gained considerable attentions of the researchers due to its many industrial and technological applications including solar central receivers exposed to winds, cooling of nuclear reactors during emergency shutdown, cooling of electronic devices by fans, and other heat exchangers placed in a low velocity environment. An example of mixed convection over a cylinder is the cooling process in heat exchangers components. A careful literature review reveals that an intensive work has been done on convection boundary layer flow over a horizontal circular cylinder. Merkin [1] was the first who initiated the study of mixed convection flow from a horizontal circular cylinder in which, he found that the separation point delays in case of heated cylinder and it comes earlier in cooling cylinder case near the lower stagnation point. Further, a detail works on mixed convection flow along a horizontal circular cylinder have been done in different investigations [2-12] by considering Newtonian and different non-Newtonian fluids.

* Corresponding author, e-mail: irfanmustafa1983@yahoo.com

Later, the study of flow and heat transfer around an elliptic cylinder has gained great importance due to the fact that it offers less resistance to the flow and heat transfer as compared to circular cylinder. The circular cylinder is a special case of an elliptic cylinder when major and minor axes are equal. The study of boundary layer flow over an elliptic cylinder is again initiated by Merkin [13]. In which, he investigated the free convection flow over a cylinder of elliptic cross-section by considering constant surface temperature and constant surface heat flux. The problem was solved using Gortler type expansion and Blasius series method. D'Alessio and Dennis [14] studied laminar forced convection flow around an elliptic cylinder. Hossain *et al*. [15] investigated thermal radiation effect on natural convection flow over cylinders of elliptic cross-section. They found that heat transfer rate in slender body become higher than that of blunt body, and this higher heat transfer rate further increase due to the effect of thermal radiation. In literature, few studies of mixed convection flow over an elliptic circular cylinder for both Newtonian and non-Newtonian fluids have been investigated and can be found in [16-19].

The analysis of unsteady flow has received considerable attention by many researchers due to its important practical applications of fluid flow in human body vessels in which reverse flow region is developed due to unsteadiness. Therefore, Jain and Goel [20] initiated numerically the unsteady laminar forced convection from a circular cylinder. Later, Jain and Lohar [21] investigated unsteady mixed convection from a horizontal circular cylinder. The study on unsteady mixed convection flow over a circular and elliptic cylinders has been extended to viscous fluids and micropolar fluid by many researchers [22-29]. Heimenz [30] was the first, who studied 2-D stagnation point flow problem and later, Eswara and Nath [31] studied unsteady mixed convection flow at a stagnation point of a 3-D body with the effects of large injection rates. Nazar *et al*. [32] studied unsteady mixed convection flow near the forward stagnation point of a 2-D body. They showed that a smooth transition occurs from the unsteady flow to a final steady-state flow. Recently, Jamaludin *et al*. [33] studied mixed convection flow over a cylinder of elliptic cross-section near a forward stagnation point. They solved the governing boundary layer equations numerically by using Keller Box method for both blunt and slender orientations. They found that separation times come early in case of slender orientation for opposing flow case.

The study of heat transfer due to radiation in mixed convection flow has many practical applications such as gas turbines, nuclear power plants, and thermal energy storage. *etc.* A detail literature survey reveals that the effect of thermal radiation over an unsteady mixed convection flow around elliptic cylinder has not yet been considered by any researcher. Therefore, we investigate the effect of thermal radiation on unsteady mixed convection flow near a forward stagnation point over a cylinder of elliptic cross-section. The governing equations are transformed into dimensionless partial differential equations, which are then solved numerically by using Keller Box method. The effects of pertinent parameters on velocity, temperature profiles, and Nusselt number are discussed through graphs and tables.

Mathematical formulation

We consider a 2-D unsteady mixed convection flow over a horizontal cylinder of elliptic cross-section near a forward stagnation point in the presence of thermal radiation. A uniform surface temperature, T_w, is considered at the surface of the elliptic cylinder and T_∞ is the temperature of ambient fluid. The origin of the co-ordinate system is considered at the lower stagnation point of the elliptic cylinder in which $\bar{x}$ co-ordinate measures the distance around the cylinder and $\bar{y}$ co-ordinate measures the distance normal to the cylinder as shown in fig. 1. We assume the free stream velocity as $0.5U_\infty$ as by Merkin [1], very far from the cylinder which impulsively starts in vertically upward direction. After using the boundary layer approximation, the governing equations of the flow problem can be written:

$$\frac{\partial \bar{u}}{\partial \bar{x}}+\frac{\partial \bar{v}}{\partial \bar{y}}=0 \tag{1}$$

$$\frac{\partial \bar{u}}{\partial \bar{t}}+\bar{u}\frac{\partial \bar{u}}{\partial \bar{x}}+\bar{v}\frac{\partial \bar{u}}{\partial \bar{y}}=\bar{u}_e(\bar{x})\frac{\mathrm{d}\bar{u}_e(\bar{x})}{\mathrm{d}\bar{x}}+\nu\frac{\partial}{\partial \bar{y}}\left(\frac{\partial \bar{u}}{\partial \bar{y}}\right)+\beta \mathrm{g}\left(T-T_\infty\right)\sin\ \varphi \tag{2}$$

$$\frac{\partial T}{\partial \bar{t}}+\bar{u}\frac{\partial T}{\partial \bar{x}}+\bar{v}\frac{\partial T}{\partial \bar{y}}=\frac{1}{\rho c_p}\frac{\partial}{\partial \bar{y}}\left\{\left[k+\frac{16\sigma T^3}{3\left(\alpha_r+\alpha_s\right)}\right]\frac{\partial T}{\partial \bar{y}}\right\} \tag{3}$$

subject to the initial and boundary conditions:

$$\begin{gathered}\bar{t}<0:\ \bar{u}\left(\bar{x},\bar{y}\right)=\bar{v}\left(\bar{x},\bar{y}\right)=0,\ T\left(\bar{x},\bar{y}\right)=T_\infty \ \text{ for any } \bar{x},\bar{y}\\ \bar{t}\geq 0:\ \bar{u}\left(\bar{x},0\right)=\bar{v}\left(\bar{x},0\right)=0,\ T\left(\bar{x},0\right)=T_w \ \text{ and } \bar{u}\left(\bar{x},\bar{y}\right)=\bar{u}_e(\bar{x}), T\left(\bar{x},\bar{y}\right)\to T_\infty \text{ as } \bar{y}\to\infty,\end{gathered} \tag{4}$$

where ($\bar{u}$, $\bar{v}$) are the velocity components in $\bar{x}$ and $\bar{y}$ directions, respectively, and φ is the angle between outward normal and downward vertical from the cylinder. The ρ is the density of the fluid, ν – the kinematic viscosity, β – the thermal expansion coefficient, g – the acceleration due to gravity, c_p – the specific heat constant, k – the thermal conductivity, T – the temperature of the fluid, σ – the Stefan-Boltzmann constant, α_r – the Rosseland mean absorption coefficient, and α_s – the scattering coefficient. The radiation effect in eq. (3) is considered by using the Rosseland diffusion approximation, Siegel and Howell [34]. Under this approximation the solution is not valid for situations where scattering is expected to be non-isotropic as well as in the immediate vicinity of the surface of the cylinder. Now introducing the non-dimensional variables as reported by Ali *et al*. [24]:

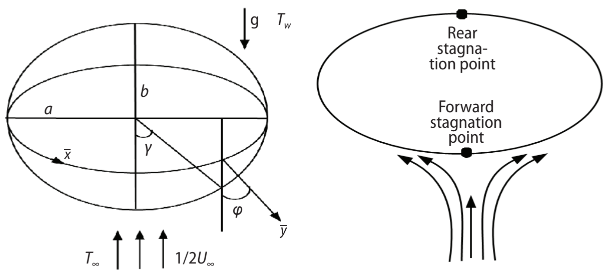

Figure 1. The physical model and co-ordinate system for the considered problem

$$x=\frac{\bar{x}}{a},\quad y=\frac{\sqrt{\mathrm{Re}}}{a}\bar{y},\quad u=\frac{\bar{u}}{U_\infty},\quad v=\sqrt{\mathrm{Re}}\left(\frac{\bar{v}}{U_\infty}\right),\quad t=\frac{U_\infty}{a}\bar{t},\quad \theta=\frac{T-T_\infty}{T_w-T_\infty} \tag{5}$$

where Re = aU_∞/ν is the Reynolds number. Using eq. (5) into the eqs. (1-3), the non-dimensional form of governing equations are:

$$\frac{\partial u}{\partial x}+\frac{\partial v}{\partial y}=0 \tag{6}$$

$$\frac{\partial u}{\partial t}+u\frac{\partial u}{\partial x}+v\frac{\partial u}{\partial y}=u_e(x)\frac{\mathrm{d}u_e(x)}{\mathrm{d}x}+\frac{\partial}{\partial y}\left(\frac{\partial u}{\partial y}\right)+\lambda\theta\sin\left(\varphi\right) \tag{7}$$

$$\frac{\partial\theta}{\partial t}+u\frac{\partial\theta}{\partial x}+v\frac{\partial\theta}{\partial y}=\frac{1}{\Pr}\frac{\partial}{\partial y}\left(\left\{1+\frac{4}{3}R_d\left[1+\left(\theta_w-1\right)\theta\right]^3\right\}\frac{\partial\theta}{\partial y}\right) \tag{8}$$

where λ = Gr/Re^2 is the mixed convection parameter, Pr = ν/α – the Prandtl number, $R_d = 4\sigma T_\infty^3/k(\alpha_r + \alpha_s)$ – the radiation parameter, Gr = $g\beta(T_w - T_\infty)a^3/\nu^2$ – the Grashof number and $\theta_w = T_w/T_\infty$ – the surface temperature parameter. It is necessary to mentioned, here, that $\lambda > 0$ corresponds to assisting flow $T_w > T_\infty$ and $\lambda < 0$ corresponds to opposing flow $T_w < T_\infty$. The initial and boundary conditions (4) take the new form:

$$\begin{gathered} t<0:\ u(x,y)=v(x,y)=0,\quad \theta(x,y)=0\quad \text{for any}\quad x,y \\ t\ge 0:\ u(x,0)=v(x,0)=0,\quad \theta(x,0)=1, \\ u(x,y)=u_e(x),\quad \theta(x,y)=0\quad \text{as}\quad y\to\infty \end{gathered} \tag{9}$$

Now introduce the following suitable transformation:

$$\psi=\sqrt{t}\,u_e(x)f(x,\eta,t),\quad \theta=\theta(x,\eta,t),\quad \eta=\frac{y}{\sqrt{t}} \tag{10}$$

Using eq. (10) into the eqs. (7) and (8), the system of dimensionless partial differential equations is obtained:

$$\begin{aligned} &\frac{\partial^3 f}{\partial\eta^3}+\frac{\eta}{2}\frac{\partial^2 f}{\partial\eta^2}+t\frac{\partial u_e}{\partial x}\left[1-\left(\frac{\partial f}{\partial\eta}\right)^2+f\frac{\partial^2 f}{\partial\eta^2}\right]= \\ &=t\frac{\partial^2 f}{\partial\eta\partial t}+tu_e\left(\frac{\partial f}{\partial\eta}\frac{\partial^2 f}{\partial\eta\partial x}-\frac{\partial f}{\partial x}\frac{\partial^2 f}{\partial\eta^2}\right)-t\lambda\theta\frac{\sin(\varphi)}{u_e} \end{aligned} \tag{11}$$

$$\begin{aligned} &\frac{1}{\Pr}\frac{\partial}{\partial\eta}\left(\left\{1+\frac{4}{3}R_d\left[1+\left(\theta_w-1\right)\theta\right]^3\right\}\frac{\partial\theta}{\partial\eta}\right)+t\frac{\partial u_e}{\partial x}f\frac{\partial\theta}{\partial\eta}+\frac{\eta}{2}\frac{\partial\theta}{\partial\eta}= \\ &=t\left[\frac{\partial\theta}{\partial t}+u_e\left(\frac{\partial f}{\partial\eta}\frac{\partial\theta}{\partial x}-\frac{\partial f}{\partial x}\frac{\partial\theta}{\partial\eta}\right)\right] \end{aligned} \tag{12}$$

the initial and boundary conditions (9) become:

$$\begin{gathered} t<0:\quad f=\frac{\partial f}{\partial\eta}=0,\quad \theta=0\quad \text{for any } x \text{ and } \eta \\ t\ge 0:\quad f=\frac{\partial f}{\partial\eta}=0,\quad \theta=1\quad \text{at } \eta=0, \\ \frac{\partial f}{\partial\eta}=1,\quad \theta=0\quad \text{as } \eta\to\infty \end{gathered} \tag{13}$$

There are two orientations for the cylinder of elliptic cross-section namely blunt orientation and slender orientation in which major axis is taken horizontally and vertically, respectively. Here x and $\sin(\varphi)$ in terms of eccentric angle γ for blunt and slender orientations are:

$$x=\int_0^{\gamma}\sqrt{(1-e^2\sin^2 z)}\,\mathrm{d}z,\quad \sin(\varphi)=\frac{b}{a}\frac{\sin\gamma}{\sqrt{1-e^2\sin^2\gamma}} \tag{14}$$

and

$$x=\int_0^{\gamma}\sqrt{(1-e^2\cos^2 z)}\,\mathrm{d}z,\quad \sin(\varphi)=\frac{\sin\gamma}{\sqrt{1-e^2\cos^2\gamma}} \tag{15}$$

respectively, where a and b are the length of semi major and minor axes and e is the eccentricity which is given by $e^2 = 1 - (b/a)^2$. In case of blunt and slender orientations, we take $\omega = b/a$ ($\omega < 1$) and $\omega = (a/b)^2$ ($\omega > 1$), respectively.

Forward stagnation point flow

In this study, we consider only the case of forward stagnation point ($x = 0$) flow over a cylinder of elliptic cross-section. The term on the RHS of eq. (11), $\sin(\varphi)/u_e$ approaches ω when x approaches zero. The potential velocity $u_e(x) = \sin(x)$ as reported by Ingham and Merkin [22] becomes zero in case of forward stagnation point and $\partial u_e/\partial x = 1$. At the forward stagnation point the governing partial differential eqs. (11) and (12) become:

$$\frac{\partial^3 f}{\partial\eta^3}+\frac{\eta}{2}\frac{\partial^2 f}{\partial\eta^2}+t\left[1-\left(\frac{\partial f}{\partial\eta}\right)^2+f\frac{\partial^2 f}{\partial\eta^2}\right]=t\frac{\partial^2 f}{\partial\eta\partial t}-t\lambda\theta\omega \tag{16}$$

$$\frac{1}{\Pr}\frac{\partial}{\partial\eta}\left(\left\{1+\frac{4}{3}R_d\left[1+\left(\theta_w-1\right)\theta\right]^3\right\}\frac{\partial\theta}{\partial\eta}\right)+tf\frac{\partial\theta}{\partial\eta}+\frac{\eta}{2}\frac{\partial\theta}{\partial\eta}=t\left(\frac{\partial\theta}{\partial t}\right) \tag{17}$$

subject to the boundary conditions:

$$\begin{gathered} t\geq 0:\quad f=\frac{\partial f}{\partial\eta}=0,\quad \theta=1\quad \text{at}\quad \eta=0,\\ \frac{\partial f}{\partial\eta}=1,\quad \theta=0\quad \text{as}\quad \eta\to\infty \end{gathered} \tag{18}$$

The physical quantities of interest are the local skin friction coefficient and Nusselt number which are defined:

$$C_f=\frac{\tau_w}{\rho_\infty U_\infty^2},\quad \mathrm{Nu}=\frac{aq_w}{k\left(T_w-T_\infty\right)} \tag{19}$$

where τ_w is the wall shear stress and q_w is the constant heat flux from the surface, which are defined:

$$\tau_w=\mu\left(\frac{\partial\bar{u}}{\partial\bar{y}}\right)_{\bar{y}=0},\quad q_w=-\left\{\left[k+\frac{16\sigma T^3}{3(\alpha_r+\alpha_s)}\right]\frac{\partial T}{\partial\bar{y}}\right\}_{\bar{y}=0} \tag{20}$$

After using eq. (20) into eq. (19), the skin friction coefficient and Nusselt number take the form:

$$C_f\sqrt{\mathrm{Re}} = \frac{1}{\sqrt{t}}u_e\frac{\partial^2 f(0,t)}{\partial\eta^2},$$

$$\frac{\mathrm{Nu}}{\sqrt{\mathrm{Re}}} = -\left(1+\frac{4}{3}R_d\theta_w^3\right)\frac{1}{\sqrt{t}}\frac{\partial\theta(0,t)}{\partial\eta}$$

The skin friction coefficient $C_f(\mathrm{Re})^{1/2}$ vanishes as $u_e(x) = 0$ at forward stagnation point.

Result and discussion

The numerical solution of non-linear partial differential equations (16) and (17) subject to the boundary conditions (18) is obtained by using implicit finite difference scheme known as Keller Box method. The method is described in detail in the book of Cebeci and Bradshaw [35]. The effects of pertinent parameters like mixed convection parameter, λ, blunt and slender orientations parameter, ω, Prandtl number, radiation parameter, R_d, and surface temperature parameter, θ_w, on the flow behavior are shown graphically by plotting velocity, temperature profiles, and Nusselt number. For the validation of our results, the values of separation times of the boundary layer flow near a forward stagnation point are compared with the work of Jamaludin *et al*. [33], as shown in tabs. 1 and 2 for the particular values of ω, λ, Pr, R_d, and θ_w. It is found that our results are in good agreement with the previous study.

Table 1. The separation times, t_s, of the cylinder of elliptic cross-section near forward stagnation point (x = 0) for Pr = 1 and λ = –3 (opposing flow)

		Blunt orientation, $\omega = b/a$				Slender orientation, $\omega = (a/b)^2$			
		0.1	0.25	0.5	0.75	100	16	4	1.7778
R_d = 0.0	t_s [33]	–	–	–	1.5210	0.00330	0.02150	0.0954	0.2652
	t_s [present]	–	–	–	1.5210	0.00335	0.02155	0.0958	0.2652
R_d = 0.5, θ_w = 1.1	t_s [present]	–	–	–	1.0225	0.0029	0.0186	0.0816	0.2192

Table 2. The separation times, t_s, of the cylinder of elliptic cross-section near forward stagnation point (x = 0) for Pr = 7 and λ = –3 (opposing flow)

		Blunt orientation, $\omega = b/a$				Slender orientation, $\omega = (a/b)^2$			
		0.1	0.25	0.5	0.75	100	16	4	1.7778
R_d = 0.0	t_s [33]	–	–	–	–	0.0060	0.0361	0.1233	0.2252
	t_s [present]	–	–	–	–	0.00613	0.0403	0.1962	0.6790
R_d = 0.5, θ_w = 1.1	t_s [present]	–	–	–	–	0.0049	0.0323	0.1512	0.4734

Table 1 presents the separation times along the elliptic cylinder near a forward stagnation point in absence as well as presence of thermal radiation for both blunt and slender orientations with the fixed values of other parameters like Pr = 1 and λ = –3 (opposing flow). In blunt orientation, separation times do not occur for values of parameter ω = 0.1, 0.25, and 0.5. In case of slender orientation, it is seen that separation time decreases with the increase of ω. It is also seen that separation time in blunt orientation is higher than slender orientation. In the presence of thermal radiation, separation times of the boundary layer flow reduce. In tab. 2, for Pr = 7, the same behavior is observed as shown in tab. 1, but in blunt orientation separation time does not occur. It is noticed that the separation times increase with the increase of Prandtl number. The variation in separation time near forward stagnation point against mixed convection parameter, λ, in the absence as well as in the presence of thermal radiation is shown in fig. 2. It is noticed that separation time decreases with the increase of absolute values of mixed convection parameter, λ. Further it is noticed that separation time reduces due to the presence of thermal radiation. The effects of involving parameters on velocity and temperature profiles for both cases of blunt and slender orientations are shown in figs. 3-10. Figures 3-6 show the velocity and temperature profiles for some values of time, t, in the absence as well as in the presence of thermal radiation parameter in which dashed lines represent thermal radiation effect. Figures 3(a) and 3(b) show velocity profiles in assisting flow case for blunt orientation (ω = 0.5) and slender orientation (ω = 4), respectively. The figs. 3(a) and 3(b) depict that the velocity increases with the increase of time, t, in both blunt and slender orientations. But in slender orientation, overshoot profile appears for t > 0.3. It can be further noted that velocity profile increases due to thermal radiation. Figures 4(a) and 4(b) show the variation in velocity

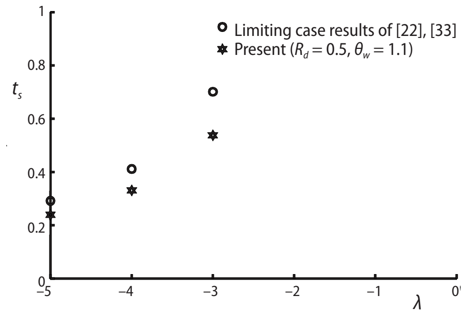

Figure 2. Variation of separation times near a forward stagnation point (x = 0) when Pr = 1, λ = –3, and ω = 1

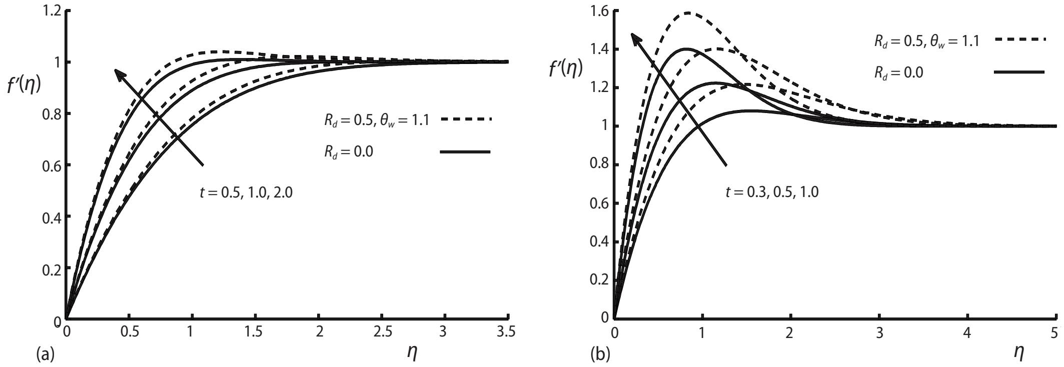

Figure 3. Velocity profiles at x = 0 (assisting flow) for various values of t when λ = 2 and Pr = 1 in: (a) blunt orientation ω = 0.5, (b) slender orientation ω = 4

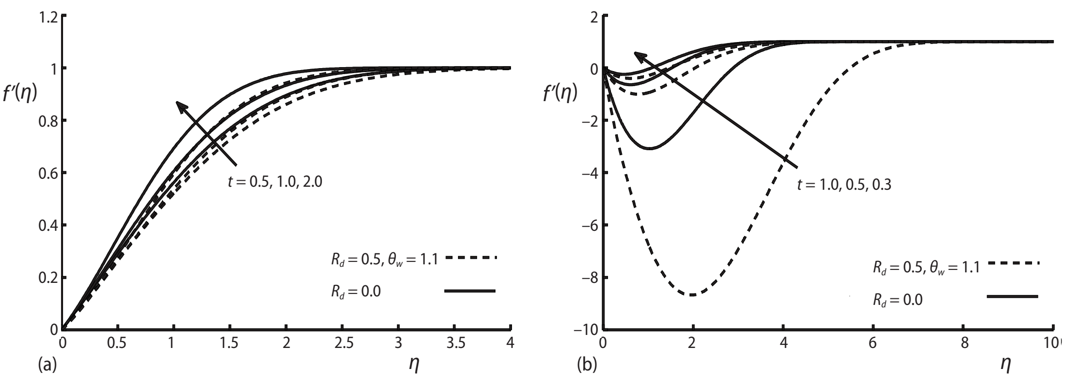

Figure 4. Velocity profiles at x = 0 (opposing flow) for various values of t when λ = –3 and Pr = 1 in: (a) blunt orientation ω = 0.5, (b) slender orientation ω = 4

profile in opposing flow case for blunt and slender orientation cases, respectively. It is seen that velocity increases in blunt orientation and decreases in slender orientation with the increase of time, t. It further shows that radiation effect reduces the velocity in both blunt and slender orientation cases. The momentum boundary layer thickness in blunt orientation decreases with the increase of time, t. Figures 5(a) and 5(b) present the temperature profiles for different values of time, t, in assisting flow both for blunt and slender orientations. It is seen that temperature and thermal boundary layer thickness decrease with the increase of time, t, in both orientations but the value of temperature increases in the presence of thermal radiation parameter.

Figures 6(a) and 6(b) are drawn to show the behavior of temperature in opposing flow case for different values of time. Figure 6(a) shows same behavior as observed in figs. 5(a) and 5(b) but the opposite behavior is observed in fig. 6(b). It shows that for large value of time, in presence of radiation effects, the heat transfer rate blows up. The effect of thermal radiation parameter, R_d,

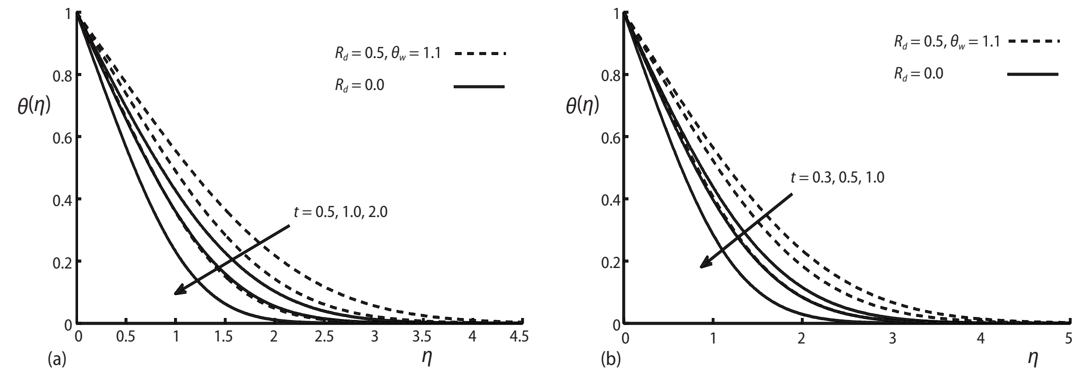

Figure 5. Temperature profiles at x = 0 (assisting flow) for various values of t when λ = 2 and Pr = 1 in: (a) blunt orientation ω = 0.5, (b) slender orientation ω = 4

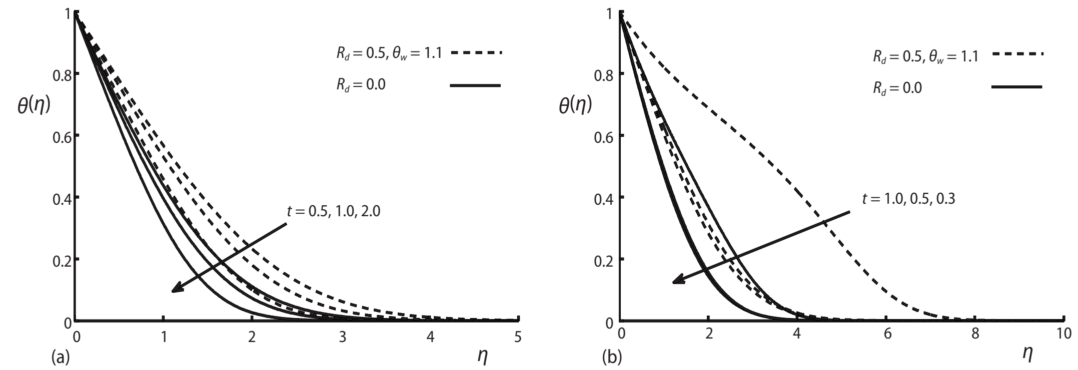

Figure 6. Temperature profiles at x = 0 (opposing flow) for various values of t when λ = –3 and Pr = 1 in: (a) blunt orientation ω = 0.5, (b) slender orientation ω = 4

on velocity and temperature profiles for both opposing and assisting flow cases are shown in figs. (7) and (8) when Pr = 1, t = 0.15, and θ_w = 1.1. The dashed and solid lines represent the solutions of blunt (ω = 0.5) orientation and slender (ω = 4) orientation, respectively. Figure 7(a) depicts that the velocity decreases in both blunt and slender orientations with the increase of thermal radiation in opposing flow case (λ = –3). It is further seen that the reverse flow occurs in slender orientation in opposing flow. Figure 7(b) shows that velocity increases in

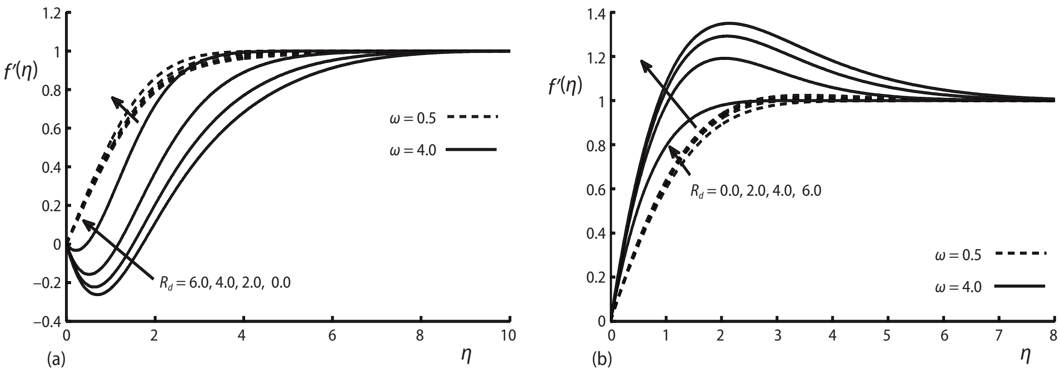

Figure 7. Velocity profiles at $x = 0$ for various values of R_d when $\theta_w = 1.1$, $t = 0.15$, and Pr = 1 in: (a) opposing flow $\lambda = -3$, (b) assisting flow $\lambda = 2$

both blunt and slender orientations with the increase of thermal radiation in assisting flow case ($\lambda = 2$). Figures 8(a) and 8(b) show that the temperature and thermal boundary layer thicknesses increase with the increase of thermal radiation parameter, R_d, both for blunt and slender orientations. In opposing flow, the value of temperature is minimum in blunt orientation as well as in slender orientation but an opposite behavior is observed in assisting flow case.

The effects of pertinent parameters on Nusselt number are plotted in figs. (9) and (10). Figures 9(a*)* and 9(b) illustrate the variation in Nusselt number against *t* for various values of ω when Pr = 1 for both blunt and slender orientations, respectively, in opposing flow case ($\lambda = -3$). Figure 9(a) shows that Nusselt number decreases in blunt orientation with the increase of ω both in the presence and in the absence of radiation effect. The transition in Nusselt number from the initial unsteady flow to the final steady flow becomes smooth but for $\omega = 0.75$ the value of Nusselt number truncates up to a certain value of, *t*, due to the separation. It is seen that radiation effect further enhances the values of Nusselt number for all time, *t*. In fig. 9(b) Nusselt number decreases in slender orientation up to certain values of *t* with the increase of ω due to the separation time and the values of heat transfer rate increase due to thermal radiation. Figures 10(a) and 10(b) demonstrate the variation in Nusselt number against *t* for various values of thermal radiation parameter, R_d, for both opposing ($\lambda = -3$) and assisting ($\lambda = 2$) flow cases, when Pr = 1 and $\theta_w = 1.1$. Nusselt number increases with the increase of thermal radiation for

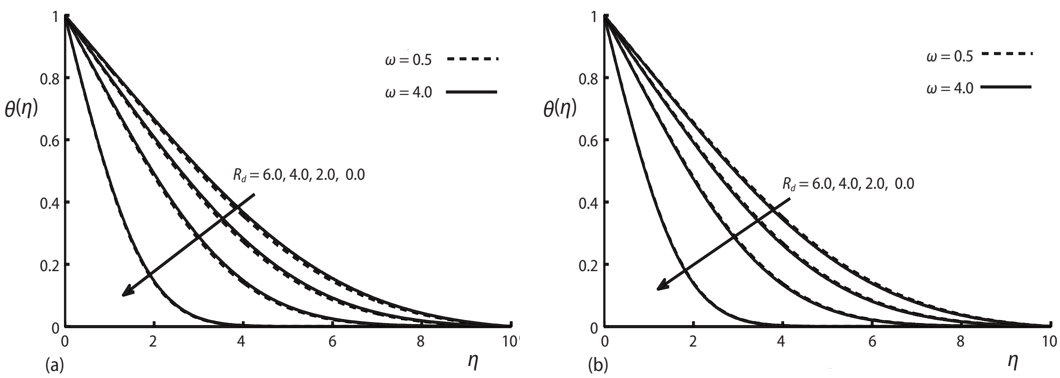

Figure 8. Temperature profiles at $x = 0$ for various values of R_d when $\theta_w = 1.1$, t = 0.15, and Pr = 1 in: (a) opposing flow $\lambda = -3$, (b) assisting flow $\lambda = 2$

both blunt and slender orientations. This is due to the fact that the increasing values of R_d help to enhance the interaction of radiation with the thermal boundary layers and, therefore, the heat absorption intensity of the fluid increases. In fig. 10(a), the values of Nusselt number in blunt orientation for $R_d < 4$ become smooth from initial unsteady flow to final steady flow but for large values of R_d Nusselt number truncates up to certain values of time due to the separation. In slender orientation the values of Nusselt number for each values of R_d truncate up to certain values of t due to the separation. In fig. 10(b) for assisting flow, the values of Nusselt number become smooth from initial unsteady flow to final steady flow in both orientations. It is further observed that heat transfer rate in slender orientation is greater than the blunt orientation.

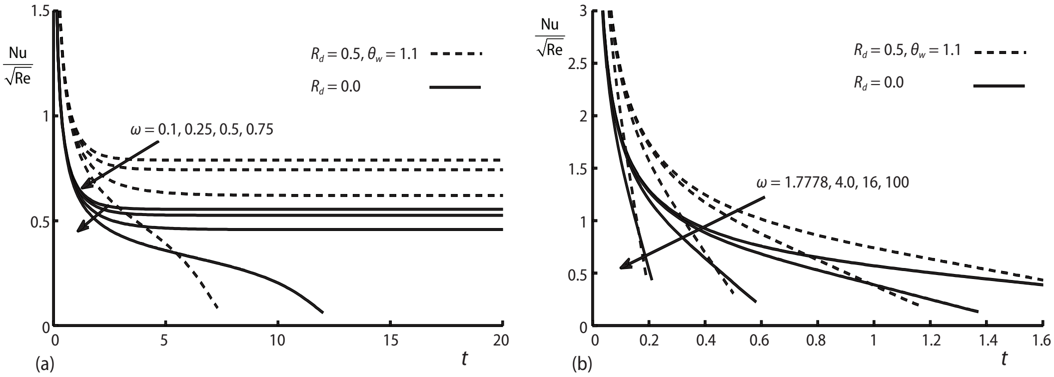

Figure 9. Variation in Nusselt number against t at $x = 0$ for various values of ω when $\lambda = -3$ and Pr = 1 in: (a) blunt orientation, (b) slender orientation

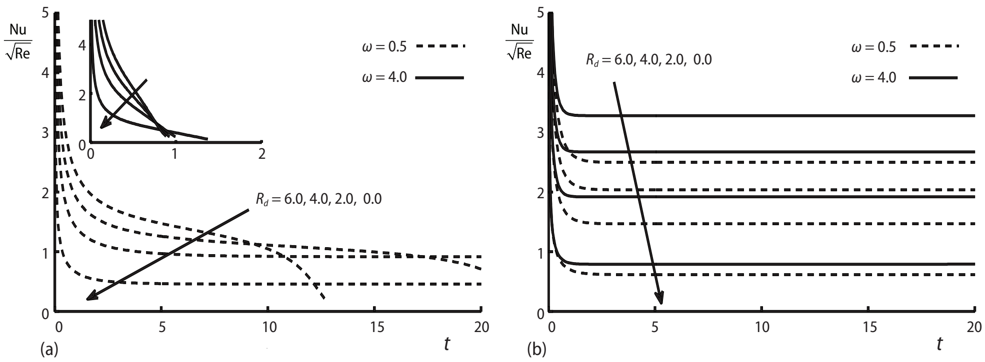

Figure 10. Variation in Nusselt number against t at $x = 0$ for various values of R_d when $\theta_w = 1.1$ and Pr = 1 in: (a) opposing flow $\lambda = -3$, (b) assisting flow $\lambda = 2$

Conclusions

In this paper, we studied the effect of thermal radiation on unsteady mixed convection flow over a cylinder of elliptic cross-section near a forward stagnation point. The separation times near the forward stagnation point in both blunt and slender orientations cases with thermal radiation effects have been calculated by using implicit finite difference scheme (Keller Box method) and are shown in tabular and graphical forms. It is observed that boundary layer separation occurs early due to of thermal radiation and the value of skin friction coefficient becomes equal to zero near a forward stagnation point. In opposing flow, the values of velocity in blunt orientation are greater than those in slender orientation due to thermal radiation and the values of temperature profile in blunt orientation are smaller than those in slender orientation. An opposite behavior is observed in assisting flow case. In opposing flow, for both blunt and slender orientations, heat transfer rate increases due to thermal radiation. The heat transfer rate in blunt orientation is greater than in slender orientation in the presence of thermal radiation in opposing flow case but an opposite behavior is observed in assisting flow.

Acknowledgement

The authors are grateful to the anonymous reviewer's valuable comments that improved the manuscript.

Nomenclature

a, b – length of semi major and minor axes, [m]
C_f – skin friction coefficient, [–]
c_p – specific heat constant, [m^{2}s^{-2}K^{-1}]
f – dimensionless stream function, [–]
g – acceleration due to gravity, [ms^{-2}]
k – thermal conductivity, [kgmT^{-3}K^{-1}]
Nu – Nusselt number, [–]
Pr – Prandtl number, [–]
q_w – wall heat flux, [kgs^{-3}]
Re – Reynolds number, [–]
R_d – thermal radiation parameter, [–]
T – temperature of the fluid in the boundary layer, [K]
T_w – surface temperature, [K]
T_∞ – ambient fluid temperature, [K]
t – time, [s]
t_s – separation times, [s]
$\bar{u}$, $\bar{v}$ – velocity components in $\bar{x}$ and $\bar{y}$ directions, respectively, [ms^{-1}]
U_∞ – free stream velocity [ms^{-1}]
$\bar{u}_e$ – potential velocity [ms^{-1}]

Greek symbols

α – thermal diffusivity, [m^{2}s^{-1}]
α_r – Rosseland mean absorption coefficient, [m^{-1}]
α_s – scattering coefficient, [m^{-1}]
β – thermal expansion coefficient, [K^{-1}]
γ – eccentric angle, [–]
η – similarity variable, [–]
θ – dimensionless temperature, [–]
θ_w – surface temperature parameter, [–]
λ – mixed convection parameter, [–]
μ – dynamic viscosity, [kgm^{-1}s^{-1}]
ν – kinematic viscosity, [m^{2}s^{-1}]
ρ – fluid density, [kgm^{-3}]
τ_w – surface shear stress, [kgs^{-2}m^{-1}]
σ – Stefan-Boltzmann constant, [kgs^{-3}K^{-4}]
φ – angle, [°]
ψ – dimensionless stream function [–]

Subscripts

w – condition at the surface
∞ – condition far away from the surface

References

[1] Merkin, J. H., Mixed Convection from a Horizontal Circular Cylinder, *Int. J. Heat Mass Transfer*, *20* (1977), 1, pp. 73-77
[2] Ingham, D. B., Pop, I., Natural Convection about a Heated Horizontal Cylinder in Porous Medium, *J. Fluid Mech*., *184* (1987), Nov., pp. 157-181
[3] Merkin, J. H., Pop, I., A Note on the Free Convection Boundary Layer on a Horizontal Circular Cylinder with Constant Heat Transfer, *Warme-und Stoffubert*, *22* (1988), 1, pp. 79-81
[4] Nazar, R., *et al*., Mixed Convection Boundary Layer Flow a Horizontal Circular Cylinder with a Constant Surface Heat Flux, *Heat Mass Transfer, 40* (2004), 3, pp. 219-227
[5] Molla, M. M., *et al*., Natural Convection Flow from an Isothermal Horizontal Circular Cylinder in Presence of Heat Generation, *Int. J. Eng. Sci*., *44* (2006), 13-14, pp. 949-958
[6] Ahmad, S., *et al*., Mixed Convection Boundary Layer Flow Past an Isothermal Horizontal Circular Cylinder with Temperature Dependent Viscosity, *Int. J. Therm. Sci*., *48* (2009), 10, pp. 1943-1948
[7] Hu, H., Koochesfahani, M. M., Thermal Effects on the Wake of a Heated Circular Cylinder Operating in Mixed Convection Regime, *J. Fluid Mech*., *685* (2011), Oct., pp. 235-270
[8] Azim, N. H. M. A., Chowdhury, M. K., MHD Conjugate Free Convection from an Isothermal Horizontal Circular Cylinder with Joule Heating and Heat Generation, *J. Comp. Methods Phys*., *2013* (2013), ID 180516
[9] Nazar, R., *et al*., Mixed Convection Boundary Layer Flow from a Horizontal Circular Cylinder in Micropolar Fluids: Case of Constant Wall Temperature, *Int. J. Numer. Methods Heat Fluid Flow*, *13* (2003), 1, pp. 86-109

[10] Anwar, I., *et al*., Mixed Convection Boundary Layer Flow of a Viscoelastic Fluid over a Horizontal Circular Cylinder, *Int. J. Nonlinear Mech*., *43* (2008), 9, pp. 814-821
[11] Srinivas, A. T., *et al*., Mixed Convection Heat Transfer from a Cylinder in Power-Law Fluids: Effect of Aiding Buoyancy, *Ind. Eng. Chem. Res*., *48* (2009), 21, pp. 9735-9754
[12] Bhowmik, S., *et al*., Non-Newtonian Mixed Convection Flow along an Isothermal Horizontal Circular Cylinder, *Numer. Heat Tr*., *A-Appl.*, *66* (2014), 5, pp. 509-529
[13] Merkin, J. H., Free Convection Boundary Layers on Cylinders of Elliptic Cross Section, *J. Heat Transfer*, *99* (1977), 3, pp. 453-457
[14] D'Alessio, S. J. D., Dennis, S. C. R., Steady Laminar Forced Convection from an Elliptic Cylinder, *J. Eng. Math*., *29* (1995), 2, pp. 181-193
[15] Hossain, M. A., *et al*., Effect of Thermal Radiation on Natural Convection over Cylinders of Elliptic Cross Section, *Acta Mech.*, *129* (1998), 3-4, pp. 177-186
[16] Cheng, C.-Y., A Boundary Layer Analysis of Heat Transfer by Free Convection from Permeable Horizontal Cylinders of Elliptic Cross Section in Porous Media Using a Thermal Non-Equilibrium Model, *Int. Commun. Heat Mass*, *34* (2007), 5, pp. 613-622
[17] Ahmad, S., *et al*., Free Convection Boundary Layer Flow over Cylinders of Elliptic Cross Section with Constant Surface Heat Flux, *Eur. J. Sci. Res*., *23* (2008), 4, pp. 613-625
[18] Cheng, C.-Y., Natural Convection Heat Transfer from a Horizontal Isothermal Elliptical Cylinder with Internal Heat Generation. *Int. Commun. Heat Mass*, *36* (2009), 4, pp. 346-350
[19] Kaprawi, S., Santoso, D., Convective Heat Transfer from a Heated Elliptic Cylinder at Uniform Wall Temperature, *IJEE*, *4* (2013), 1, pp. 133-140
[20] Jain, P. C., Goel, B. S., A Numerical Study of Unsteady Laminar Forced Convection from a Circular Cylinder, *J. Heat Transfer, 98* (1976), 2, pp. 303-307
[21] Jain, P. C., Lohar, B. L., Unsteady Mixed Convection Heat Transfer from a Horizontal Circular Cylinder, *J. Heat Transfer, 101* (1979), 1, pp. 126-131
[22] Ingham, D. B., Merkin, J. H., Unsteady Mixed Convection from an Isothermal Circular Cylinder, *Acta Mech*., *38* (1981), 1-2, pp. 55-69
[23] Kamrujjaman, M., *et al*., Oscillating Free Convection Flow along a Heated Horizontal Circular Cylinder, *Proceedings*, Applied Mathematics and Mathematical Physics Conference, Sylhet, Bangladesh, 2005
[24] Ali, A., *et al*., Unsteady Mixed Convection Boundary Layer from a Circular Cylinder in a Micropolar Fluid, *Int. J. Chem. Eng., 2010* (2010), ID 417875
[25] Boričić, A. Z., *et al*., MHD Effects on Unsteady Dynamic, Thermal and Diffusion Boundary Layer Flow over a Horizontal Circular Cylinder, *Thermal Science*, *16* (2012), 2, pp. 311-321
[26] Chandna, A., Flow Past an Elliptic Cylinder, *J. Comput. Appl. Math*., *85* (1997), 2, pp. 203-214
[27] D'Alessio, S. J. D., Steady and Unsteady Forced Convection Past an Inclined Elliptic Cylinder, *Acta Mech*., *123* (1997), 1-4, pp. 99-115
[28] Williams, M. L., Analytic Study of Unsteady Free Convection from an Inclined Elliptic Cylinder, M. Math. Sc. thesis, Waterloo University, Waterloo, Ont., Canada, 2004
[29] Jaman, M. K., Hossain, M. A., Effect of Fluctuating Surface Temperature on Natural Convection Flow over Cylinders of Elliptic Cross Section, *Int. J. Transp. Phenom*., *2* (2010), 35, pp. 35-47
[30] Hiemenz, K., The Boundary Layer on a Straight Circular Cylinder Immersed in the Uniform Liquid Stream, *Dingler's Poly. J*., *326* (1911), pp. 321-324
[31] Eswara, A. T., Nath, G., Effect of Large Injection Rates on Unsteady Mixed Convection Flow at a Three Dimensional Stagnation Point, *Int. J. Non Linear Mech*., *34* (1999), 1, pp. 85-103
[32] Nazar, R., *et al*., Unsteady Mixed Convection Near the Forward Stagnation Point of a Two Dimensional Symmetric Body, *Int. Comm. Heat Mass Transfer*, *30* (2003), 5, pp. 673-682
[33] Jamaludin, M., *et al*., Unsteady Mixed Convection Flow over a Cylinder of Elliptic Cross Section Near Forward Stagnation Point, *Matematika*, *28* (2012), 2, pp. 109-125
[34] Siegel, R., Howell, J. R., *Thermal Radiation Heat Transfer*, McGraw-Hill, New York, USA, 1987
[35] Cebeci, T., Bradshaw, P., *Physical and Computational Aspects of Convective Heat Transfer*, Springer, New York, USA, 1984

Paper submitted: September 26, 2014
Paper revised: February 2, 2015
Paper accepted: February 16, 2015